Tulips R University of Tsukuba Repository

Lattice and grain-boundary diffusions of impurity atoms in BaSi2 epitaxial layers grown by molecular beam epitaxy

著者別名	都甲 薫, 末益 崇
journal or publication title	Journal of crystal growth
volume	378
page range	189-192
year	2013-09
権利	(C) 2013 Elsevier B.V. NOTICE: this is the author's version of a work that was accepted for publication in Journal of crystal growth. Changes resulting from the publishing process, such as peer review, editing, corrections, structural formatting, and other quality control mechanisms may not be reflected in this document. Changes may have been made to this work since it was submitted for publication. A definitive version was subsequently published in Journal of crystal growth, 378, 2013 http://dx.doi.org/10.1016/j.jcrysgro.2012.12.051
URL	http://hdl.handle.net/2241/119792

doi: 10.1016/j.jcrysgro.2012.12.051

Lattice and grain-boundary diffusions of impurity atoms in $BaSi_2$ epitaxial layers grown by molecular beam epitaxy

K. Nakamura[a], K. Toh[a], M. Baba[a], M. Ajmal Khan[a], W. Du[a], K. Toko[a], and T. Suemasu[a,b]

[a]*Institute of Applied Physics, University of Tsukuba, Tsukuba, Ibaraki 305-8573, Japan*

[b]*Japan Science and Technology Agency, CREST, Tokyo 102-0075, Japan*

Corresponding author: T. Suemasu

Institute of Applied Physics, University of Tsukuba, Tsukuba, Ibaraki 305-8573, Japan

TEL/FAX: +81-29-853-5111, Email: suemasu@bk.tsukuba.ac.jp

Abstract

Al or B layers of a few hundreds of nm in thickness deposited on $BaSi_2$ epitaxial films on Si(111) substrates were annealed at different temperatures, and the diffusion coefficients of Al and B were evaluated using secondary ion mass spectrometry with O^{2+}. We also investigated the effect of post annealing (850 ºC, 10 min) of $BaSi_2$ films on the diffusion coefficients. It was found that both the lattice diffusion and the grain boundary diffusion were decreased by the post-annealing. The plan-view transmission electron microscopy images revealed that the grain size was increased from approximately 0.2 to 0.6 μm by the annealing, and the X-ray diffraction intensities also increased. The activation energies of lattice and grain boundary diffusions in the post-annealed $BaSi_2$ are 0.63 eV and 0.58 eV for Al, and 4.6 eV and 4.4 eV for B, respectively.

PACS: 78.40.Fy

Keywords: A1. Impurity diffusion; A3. Molecular beam epitaxy; B1. Semiconducting silicides; B3. Solar cell

1. Introduction

Photovoltaic cell production has been increasing and its market continues to rapidly expand. Approximately 90% of solar cells are made from Si, because Si is an abundant and well-known material in the semiconductor industry. However, the optical absorption layers of crystalline Si (c-Si) solar cells tend to be much thicker than conventional thin-film solar cells, such as CIGS, because the optical absorption coefficient is much smaller for c-Si. Therefore, new materials for high-efficiency thin-film solar cells are of significant interest. Among such materials, we have focused on semiconducting orthorhombic $BaSi_2$, which has particularly favorable characteristics for solar cell applications. $BaSi_2$ has a bandgap of approximately 1.3 eV and a very large optical absorption coefficient, reaching 3×10^4 cm^{-1} at 1.5 eV experimentally [1-3]. *a*-Axis-oriented $BaSi_2$ can be grown epitaxially on Si(111) and S(001) substrates [4-7]. Recently, we successfully achieved large photoresponsivity and internal quantum efficiency exceeding 70% in *a*-axis-oriented $BaSi_2$ epitaxial layers grown by molecular beam epitaxy (MBE) [8-11]. These results have spurred interest in this material.

The basic structure of a solar cell is a *p-n* junction. Therefore, control of the conductivity of $BaSi_2$ by impurity doping is a requirement. The carrier concentration of undoped *n*-$BaSi_2$ is approximately 5×10^{15} cm^{-3} [1]. According to Imai and Watanabe [12], substitution of Si in the $BaSi_2$ lattice is more favorable than substitution of Ba from an energetic point of view by first-principles calculation. In our previous works, the electron

concentration of Sb-doped $BaSi_2$ was controlled in the range between 10^{16} and 10^{20} cm^{-3} at room temperature (RT). In contrast, Al- and In-doped $BaSi_2$ show *p*-type conductivity, but the hole concentration was limited up to 3×10^{17} cm^{-3} [13]. Very recently, we have achieved the hole concentration exceeding 10^{19} cm^{-3} in B-doped $BaSi_2$ [14]. Thus, the remaining step is to grow high-quality *p*-type $BaSi_2$ layers on undoped *n*-type $BaSi_2$ layers to form a $BaSi_2$ *p-n* junction. For this purpose, impurity dopants with smaller diffusion coefficient are favorable to realize a very sharp *p-n* junction. However, there have been no reports on diffusion coefficients of impurity atoms in $BaSi_2$.

In this study, we aimed to evaluate the lattice diffusion coefficient of *p*-type dopants Al and B using secondary ion mass spectrometry (SIMS) measurement. Grain boundary (GB) diffusion coefficients were also evaluated because GBs exist in the $BaSi_2$ epitaxial layers on Si(111) due to three epitaxial variants rotated by 120º around the surface normal [6,15].

2. Experimental

A two-step growth method was adopted including reactive deposition epitaxy (RDE; Ba deposition on hot Si) for $BaSi_2$ template layers, and subsequent MBE (codeposition of Ba and Si on Si) at 600 ºC to form $BaSi_2$ epitaxial films on Si(111). Details of the growth procedure have been previously described [6,15].

First, we investigated the post-annealing duration. It is well known that the crystal

quality and electrical properties of MBE-grown β-$FeSi_2$ films are improved significantly by annealing at temperatures higher than 800 ºC [16,17]. Thus, we performed post-annealing in an ultrahigh-vacuum (UHV) chamber at 850 ºC for up to 60 min to determine the proper annealing duration. From the θ-2θ X-ray diffraction (XRD) patterns, we chose to adopt 850 ºC for 10 min. The grain size of $BaSi_2$ was evaluated by plan-view transmission electron microscopy (TEM).

We next investigated the diffusion coefficients using as-grown and post-annealed (850 ºC, 10 min) $BaSi_2$ epitaxial films on Si(111). Al or B layers of a few hundreds of nm in thickness were deposited on undoped $BaSi_2$ layers at RT. These samples were cut into several pieces and annealed at different temperatures of 300, 400 and 500 °C for 6, 3 and 1 h, respectively, for Al. On the other hand, the diffusion coefficients of B were evaluated only on the post-annealed $BaSi_2$. The diffusion coefficients of B were found to be much smaller than those of Al as described later, and thus the annealing for B diffusion was necessary to perform at much higher temperatures such as 775, 800 and 825 °C for 5, 1 and 0.5 h, respectively. These temperatures were close to the post-annealing temperature of 850 °C. Thus, we omitted the evaluation of diffusion coefficients of B in the as-grown $BaSi_2$. We investigated the depth profiles of Al and B in $BaSi_2$ using SIMS measurement with O^{2+}, and evaluated the lattice and GB diffusion coefficients of Al and B atoms.

3. Results and discussion

Figure 1 shows the θ-2θ XRD patterns of as-grown and post-annealed $BaSi_2$ films at 850 ºC for 10 and 60 min. The peak intensities of the $BaSi_2$ annealed at 850 ºC for 10 min was the largest. The fact that the XRD peak intensities decreased after the 60 min annealing is probably because some amounts of Ba in the $BaSi_2$ diffused out due to its large vapor pressure during the long-time annealing. From these results, we chose to adopt the post-annealing duration as 10 min. In order to investigate what happened in the $BaSi_2$ by the post-annealing, we performed plan-view TEM observations. Figures 2(a) and 2(b) show the plan-view bright-field (BF) TEM images of the as-grown and the post-annealed $BaSi_2$ films, respectively. The incident electron beam was almost parallel to the $BaSi_2$[100] zone axis, but was slightly tilted for the GBs to be seen clearly. Note that approximately 120° sharp GBs are present. Detailed discussions about the GBs were given in our previous report [15]. We can see that the grain size of $BaSi_2$ extended by the post-annealing from approximately 0.2 to 0.6 μm. On the basis of these results, we can say that the post-annealing improved not only the crystalline quality of $BaSi_2$, but also increased the grains of $BaSi_2$.

We next discussed the diffusion coefficients of Al and B in $BaSi_2$. The depth profiles of Al and B are shown in Figs. 3(a)-3(c). Reference samples with a controlled number of Al and B doped in $BaSi_2$ have not yet been prepared but will be necessary to precisely determine the impurity concentration by SIMS. Although exact Al and B concentrations could not be

obtained, it does not affect the following analysis. From Figs. 3(a) and 3(b), it can safely be stated that the diffusion coefficients of B were much smaller than those of Al, and that the diffusion of Al was suppressed by the post-annealing. In order to fit the experimental SIMS profiles, both lattice and GB diffusions were taken into consideration because we can see clear GBs in the $BaSi_2$ films in Figs. 2(a) and 2(b). We adopted Eqs. (1) and (2) for fitting the experimentally obtained SIMS profiles. The concentration distribution $C(x,t)$ of impurity atom due to the lattice diffusion is given by Eq. (1),

$$C(x,t) = C_0 \mathrm{erfc}(x / 2\sqrt{D_l t}) \quad (1),$$

where x=0 is set at the Al(B)/$BaSi_2$ interface, and C_0 the Al(B) concentration at x=0, D_l the lattice diffusion coefficient, and t the annealing duration. On the other hand, the concentration distribution due to GB diffusion follows Eq. (2) [18],

$$s\delta D_{\mathrm{GB}} = 1.332\left(D_l / t\right)^{1/2}\left(-\partial \ln C(x,t) / \partial x^{6/5}\right)^{-5/3} \quad (2),$$

where s is the segregation factor, δ the grain boundary width, and D_{GB} the GB diffusion coefficient. Figure 4 is an example of the measured and simulated SIMS profiles of Al in the post-annealed $BaSi_2$ film. Annealing for Al diffusion was performed at 300 ℃ for 6 h in Fig. 4. The experimentally obtained depth profile of Al was reproduced relatively well with Eqs. (1) and (2). Note that there are three regions in Fig. 4; the Al layer region, the lattice diffusion region (broken line), and the GB diffusion region (dotted line). Similar fittings were performed for the other samples to evaluate the diffusion coefficients.

The Arrhenius plots for the obtained lattice diffusion coefficient D_{Lattice} and the product of segregation factor, GB width and GB diffusion coefficient $s\delta D_{GB}$ of Al and B atoms are shown in Figs. 5(a) and 5(b), respectively. In the case of Al diffusion performed on the as-grown $BaSi_2$ at temperatures higher than 400 ºC, it was difficult to fit the experimental profile using the GB diffusion because the two regions of the lattice and GB diffusions were merged. It was found from Figs. 5(a) and 5(b) that the lattice and GB diffusion coefficients of B are much smaller than those of Al, and that the post-annealing suppressed the diffusion of Al. The gradient of the Arrhenius plots in Figs. 5(a) and 5(b) revealed that the activation energies of lattice diffusion of Al and B in the post-annealed $BaSi_2$ are 0.63 eV and 4.6 eV, respectively, while those of GB diffusion are 0.58 eV and 4.4 eV, respectively. On the basis of these results, we concluded that B is a favorable dopant impurity atom from the view point of its small diffusion coefficients.

4. Summary

The lattice and GB diffusion coefficients of Al and B atoms were evaluated using the $BaSi_2$ epitaxial films capped with Al (B) layers. The post-annealing at 850 ºC for 10 min increased the grains of $BaSi_2$ from approximately 0.2 to 0.6 μm. The SIMS depth profiles of Al and B atoms were reproduced relatively well by taking both the lattice and GB diffusions into consideration. The diffusion coefficients of B were much smaller than those of Al,

meaning that B is more favorable than Al as a *p*-type dopant. The activation energies of lattice diffusion of Al and B in the post-annealed $BaSi_2$ are 0.63 eV and 4.6 eV, respectively, while those of GB diffusion are 0.58 eV and 4.4 eV, respectively.

Acknowledgements

The authors thank Mr. Saito and Ms. Yoshizawa of the National Institute of Advanced Industrial Science and Technology for plan-view TEM observation. This work was supported in part by CREST of JST.

References

[1] K. Morita, Y. Inomata, T. Suemasu, Thin Solid Films 508 (2006) 363.

[2] D. B. Migas, V. L. Shaposhnikov, V.E. Borisenko,Phys. Status Solidi B 244 (2007) 2611.

[3] K. Toh, T. Saito, T. Suemasu, Jpn. J. Appl. Phys. 50 (2011) 068001.

[4] R. A. Mckee, F. J. Walker, J. R. Conner, E. D. Specht, D. E. Zelmon, Appl. Phys. Lett. 59 (1991) 782.

[5] R. A. Mckee, F. J. Walker, Appl. Phys. Lett. 63 (1993) 2818.

[6] Y. Inomata, T. Nakamura, T. Suemasu, F. Hasegawa, Jpn. J. Appl. Phys. 43 (2004) L478.

[7] K. Toh, K. O. Hara, N. Usami, N. Saito, N. Yoshizawa, K. Toko, T. Suemasu, J. Cryst. Growth 345 (2012) 16.

[8] W. Du, M. Suzuno, M. A Khan, K. Toh, M. Baba, K. Nakamura, K. Toko, N. Usami, T. Suemasu, Appl. Phys. Lett. 100 (2012) 152114.

[9] Y. Matsumoto, D. Tsukada, R. Sasaki, M. Takeishi, T. Suemasu, Appl. Phys. Express 2 (2009) 021101.

[10] D. Tsukada, Y. Matsumoto, R. Sasaki, M. Takeishi, T. Saito, N. Usami, T. Suemasu, Appl. Phys. Express 2 (2009) 051601.

[11] T. Saito, Y. Matsumoto, M. Suzuno, M. Takeishi, R. Sasaki, N. Usami, T. Suemasu, Appl. Phys. Express 3 (2009) 021301.

[12] Y. Imai, A. Watanabe, Intermetallics 15 (2007) 1291.

[13] M. Kobayashi, Y. Matsumoto, Y. Ichikawa, D. Tsukada, T. Suemasu, Appl. Physics Express 1 (2008) 051403.

[14] M. Ajmal Khan, K O. Hara, K. Nakamura, M. Baba, K. Toh, M. Suzuno, K. Toko, N. Usami, T. Suemasu, International Conference of Molecular Beam Epitaxy, WeA-1-2, Nara, Japan, Sept.26, 2012.

[15] M. Baba, K. Toh, K. Toko, N. Saito, N. Yoshizawa, K. Jiptner, T. Sekiguchi, K. O Hara, N. Usami, T. Suemasu, J. Cryst. Growth 348 (2012) 75.

[16] M. Takauji, N. Seki, T. Suemasu, F. Hasegawa, J. Appl. Phys. 96 (2004) 2561.

[17] M. Suzuno, Y. Ugajin, S. Murase, T. Suemasu, M. Uchikoshi, M. Isshiki, J. Appl. Phys. 120 (2007) 103706.

[18] A. D. Le Claire, Br. J. Appl. Phys. 14 (1963) 351.

Figure 1 θ-2θ XRD patterns of as-grown, and annealed $BaSi_2$ films at 850 ºC for 10 or 60 min.

Figure 2 Plan-view BF TEM images of (a) as-grown and (b) post-annealed $BaSi_2$ films. The incident electron beam was almost parallel to the $BaSi_2$[100] zone axis, but was slightly tilted for the GBs to be seen clearly.

Figure 3 SIMS depth profiles of Al for (a) as-grown, (b) post-annealed $BaSi_2$ films. (c) SIMS depth profile of B for annealed $BaSi_2$ films.

Figure 4 Measured and simulated SIMS profiles of Al in the post-annealed $BaSi_2$ film. Annealing for Al diffusion was performed at 300 ºC for 6 h.

Figure 5 Arrhenius plots of (a) D_{Lattice} and (b) $s\delta D_{\mathrm{GB}}$ for as-grown and post-annealed $BaSi_2$.

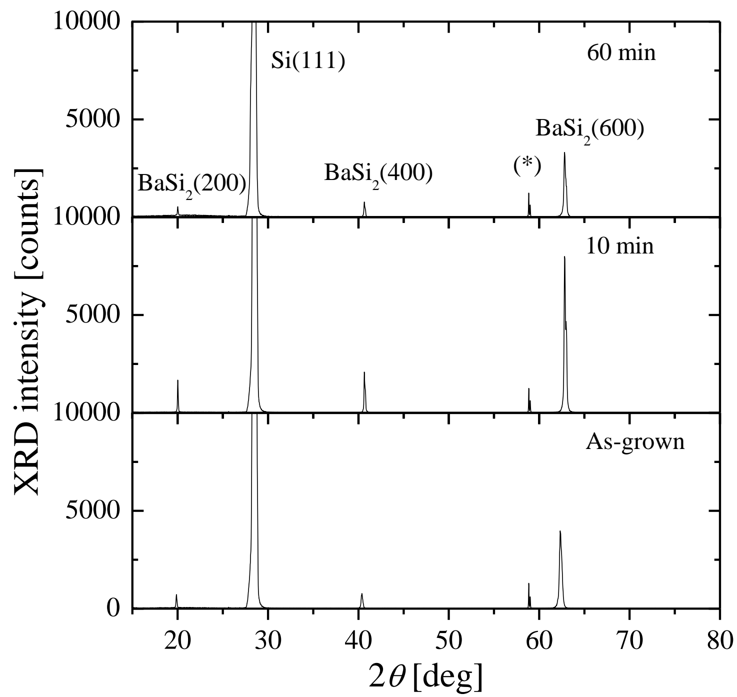

Fig. 1

a

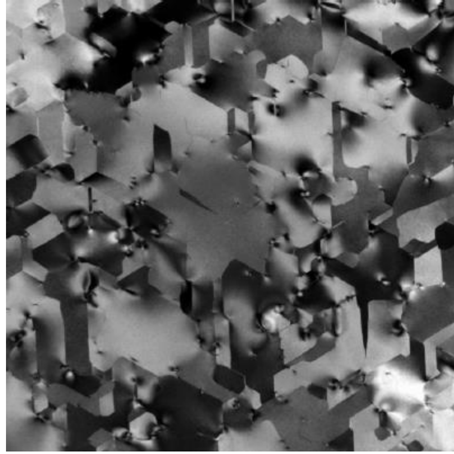

b

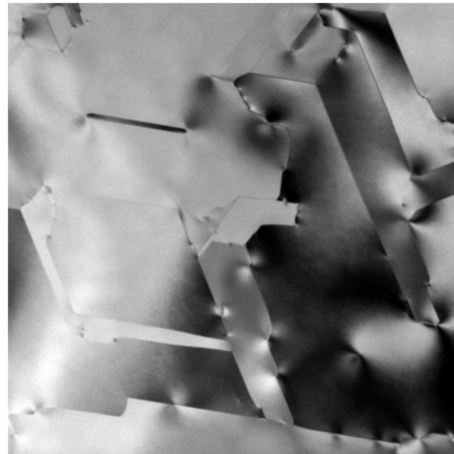

Fig. 2

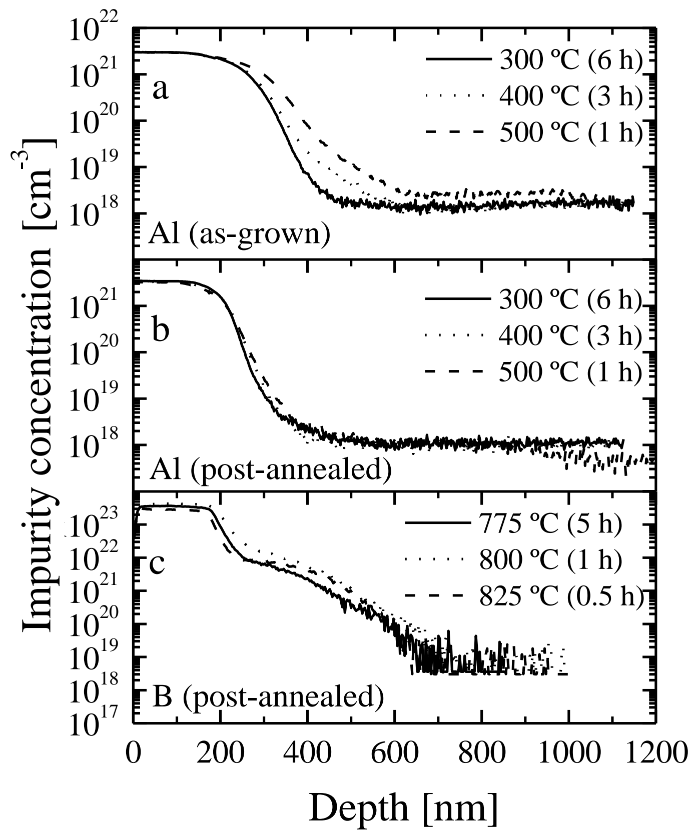

Fig. 3

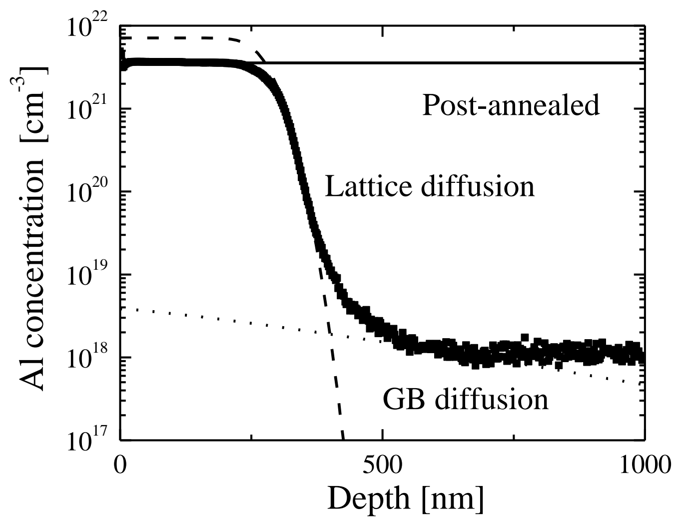

Fig. 4

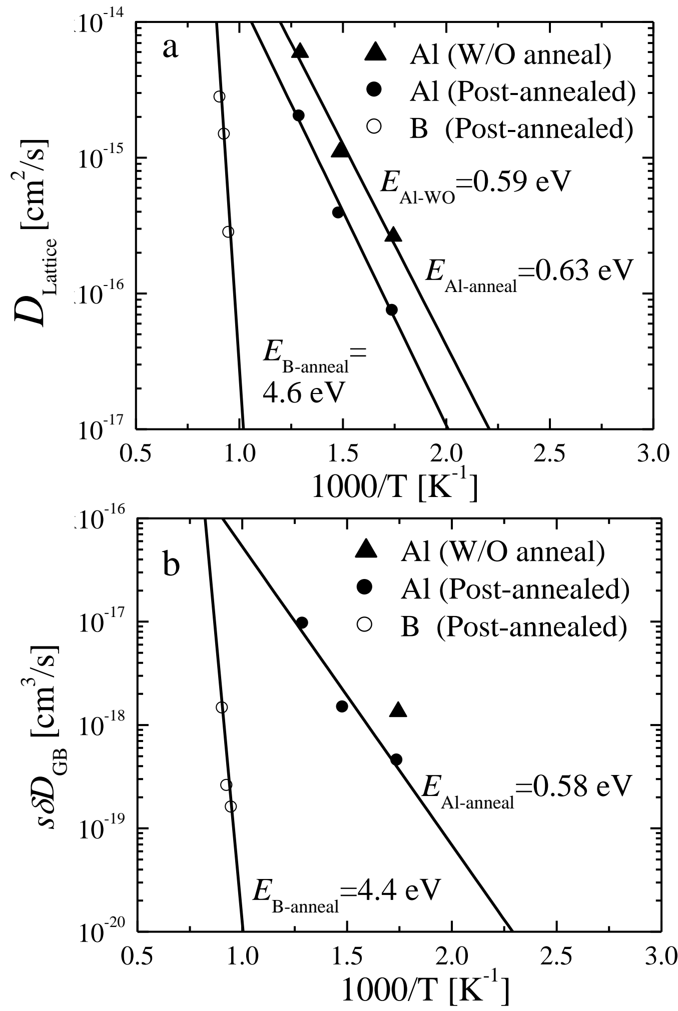

Fig. 5